NASA/TM-2021-104606/Vol. 56

Technical Report Series on Global Modeling and Data Assimilation, Volume 56

Randal D. Koster, Editor

Validation Assessment for the Soil Moisture Active Passive (SMAP) Level 4 Carbon (L4_C) Data Product Version 5

John S. Kimball, K. Arthur Endsley, Tobias Kundig, Joseph Glassy, Rolf H. Reichle and Joseph V. Ardizzone

June 2021

NASA STI Program ... in Profile

Since its founding, NASA has been dedicated to the advancement of aeronautics and space science. The NASA scientific and technical information (STI) program plays a key part in helping NASA maintain this important role.

The NASA STI program operates under the auspices of the Agency Chief Information Officer. It collects, organizes, provides for archiving, and disseminates NASA's STI. The NASA STI program provides access to the NTRS Registered and its public interface, the NASA Technical Reports Server, thus providing one of the largest collections of aeronautical and space science STI in the world. Results are published in both non-NASA channels and by NASA in the NASA STI Report Series, which includes the following report types:

- TECHNICAL PUBLICATION. Reports of completed research or a major significant phase of research that present the results of NASA Programs and include extensive data or theoretical analysis. Includes compilations of significant scientific and technical data and information deemed to be of continuing reference value. NASA counterpart of peer-reviewed formal professional papers but has less stringent limitations on manuscript length and extent of graphic presentations.

- TECHNICAL MEMORANDUM. Scientific and technical findings that are preliminary or of specialized interest, e.g., quick release reports, working papers, and bibliographies that contain minimal annotation. Does not contain extensive analysis.

- CONTRACTOR REPORT. Scientific and technical findings by NASA-sponsored contractors and grantees.

- CONFERENCE PUBLICATION. Collected papers from scientific and technical conferences, symposia, seminars, or other meetings sponsored or co-sponsored by NASA.

- SPECIAL PUBLICATION. Scientific, technical, or historical information from NASA programs, projects, and missions, often concerned with subjects having substantial public interest.

- TECHNICAL TRANSLATION. English-language translations of foreign scientific and technical material pertinent to NASA's mission.

Specialized services also include organizing and publishing research results, distributing specialized research announcements and feeds, providing information desk and personal search support, and enabling data exchange services.

For more information about the NASA STI program, see the following:

- Access the NASA STI program home page at http://www.sti.nasa.gov

- E-mail your question to help@sti.nasa.gov

- Phone the NASA STI Information Desk at 757-864-9658

- Write to:
  NASA STI Information Desk
  Mail Stop 148
  NASA Langley Research Center
  Hampton, VA 23681-2199

NASA/TM-2021-104606/Vol. 56

Technical Report Series on Global Modeling and Data Assimilation, Volume 56

Randal D. Koster, Editor

Validation Assessment for the Soil Moisture Active Passive (SMAP) Level 4 Carbon (L4_C) Data Product Version 5

John S. Kimball
University of Montana, Missoula, MT

K. Arthur Endsley
University of Montana, Missoula, MT

Tobias Kundig
University of Montana, Missoula, MT

Joseph Glassy
Lupine Logic, Inc., Missoula, MT

Rolf H. Reichle
NASA Goddard Space Flight Center, Greenbelt, MD

Joseph V. Ardizzone
Science Systems and Applications Inc., Lanham, MD

National Aeronautics and Space Administration

Goddard Space Flight Center
Greenbelt, Maryland 20771

June 2021

Level of Review: This material has been technically reviewed by technical management.

Available from

NASA STI Program
Mail Stop 148
NASA's Langley Research
Center Hampton, VA
23681-2199

National Technical Information
Service 5285 Port Royal Road
Springfield, VA 22161
703-605-6000

Table of Contents

1 EXECUTIVE SUMMARY

The post-launch Cal/Val phase of the SMAP mission is guided by two primary objectives for each science product team: 1) to calibrate, verify, and improve the performance of the science algorithms, and 2) validate accuracies of the science data products as specified in the SMAP Level-1 mission science requirements. Algorithm science and product maintenance activities during the SMAP extended mission phase have also involved periodic algorithm calibration and product refinements to maintain or enhance product consistency and performance as well as science utility. This report provides an assessment of the latest (Version 5) SMAP Level 4 Carbon (L4_C) product. The L4_C Version 5 (v5) global record now spans more than six years (March 2015 – present) of SMAP operations and has benefited from five major reprocessing updates to the operational product. These reprocessing events and L4_C product release updates have incorporated various algorithm refinements and calibration adjustments to account for similar refinements to the upstream GEOS land model assimilation system, SMAP brightness temperatures, and MODIS vegetation inputs used for L4_C processing.

The SMAP L4_C algorithms utilize a terrestrial carbon flux model informed by daily surface and root zone soil moisture information contributed from the SMAP Level 4 Soil Moisture (L4_SM) product along with optical remote sensing-based (e.g. MODIS-based) land cover and canopy fractional photosynthetic active radiation (fPAR), and other ancillary biophysical data. The carbon flux model estimates global daily net ecosystem CO_2 exchange (NEE) and the component carbon fluxes, namely, vegetation gross primary production (GPP) and soil heterotrophic respiration (R_h). Other L4_C product elements include surface (~0-5 cm depth) soil organic carbon (SOC) stocks and associated environmental constraints to these processes, including soil moisture-related controls on GPP and ecosystem respiration (Kimball et al. 2014, Jones et al. 2017). The L4_C product addresses SMAP carbon cycle science objectives by: 1) providing a direct link between terrestrial carbon fluxes and underlying freeze/thaw and soil moisture-related constraints to these processes, 2) documenting primary connections between terrestrial water, energy and carbon cycles, and 3) improving understanding of terrestrial carbon sink activity.

The SMAP L4_C algorithms and operational product are mature and at a CEOS Validation Stage 4 level (Jackson et al. 2012) based on extensive validation of the multi-year record against a diverse array of independent benchmarks, well characterized global performance, and systematic refinements gained from five major reprocessing events. There are no Level-1 mission science requirements for the L4_C product; however, self-imposed requirements have been established focusing on NEE as the primary product field for validation, and on demonstrating L4_C accuracy and success in meeting product science requirements (Jackson et al. 2012). The other L4_C product fields also have strong utility for carbon science applications (e.g., Liu et al. 2019, Endsley et al. 2020); however, analysis of these other fields is considered secondary relative to primary validation activities focusing on NEE. The L4_C targeted accuracy requirements are to meet or exceed a mean unbiased root-mean-square error (ubRMSE, or standard deviation of the error) for NEE of 1.6 g C m^{-2} d^{-1} and 30 g C m^{-2} yr^{-1}, emphasizing northern (≥45°N) boreal and arctic ecosystems; this accuracy is similar to that of tower eddy covariance measurement-based observations (Baldocchi 2008).

Methods used for the latest v5 L4_C product performance and validation assessment have been established from the SMAP Cal/Val plan and previous studies (Jackson et al. 2012, Jones et al. 2017) and include: 1) consistency evaluations of the product fields against earlier product releases (version 4 or earlier); 2) comparisons of daily carbon flux estimates with independent tower eddy

covariance measurement-based daily carbon (CO_2) flux observations from core tower validation sites (CVS); and 3) consistency checks against other global carbon products, including soil carbon inventory records, global GPP records derived from tower observation upscaling methods, and satellite-based observations of canopy solar induced chlorophyll fluorescence (SIF) as a surrogate for GPP. Metrics used to evaluate relative agreement between L4_C product fields and observational benchmarks include correlation (r-value), RMSE differences, bias and model sensitivity diagnostics. Following these validation criteria, the present report provides a validation assessment of the latest L4_C product release (v5). Detailed descriptions of the L4_C algorithm and additional global product accuracy and performance results are given elsewhere (Jones et al. 2017, Endsley et al. 2020).

The v5 L4_C product replaces earlier product versions and continues to show: (i) accuracy and performance levels meeting or exceeding SMAP L4_C science requirements; (ii) improvement over the previous product version (version 4); and (iii) suitability for a diversity of science applications. Example L4_C applications from the recent literature include clarifying environmental trends and controls on the northern terrestrial carbon sink (Liu et al. 2019), diagnosing drought-related impacts on ecosystem productivity (Li et al. 2020), and regional monitoring of cropland conditions for projecting annual yields (Wurster et al. 2020).

2 EXPECTED L4_C ALGORITHM AND PRODUCT PERFORMANCE

The L4_C algorithm performance, including variance and uncertainty estimates of model outputs, was determined during the mission pre-launch phase through spatially explicit model sensitivity studies using available model inputs similar to those currently being used for operational production and evaluating the resulting model simulations over the observed range of northern (≥45 °N) and global conditions (Kimball et al. 2012, Entekhabi et al. 2014). The L4_C algorithm options were also evaluated during the mission prelaunch phase, including deriving canopy fPAR from lower order NDVI (Normalized Difference Vegetation Index) inputs in lieu of using MODIS (MOD15) fPAR; and including an explicit model representation of boreal fire disturbance recovery impacts. These results indicated that the L4_C accuracy requirements (i.e., NEE ubRMSE ≤ 30 g C m^{-2} yr^{-1} or ≤ 1.6 g C m^{-2} d^{-1}) could be met from the baseline algorithms over more than 82% and 89% of global and northern vegetated land areas, respectively (Yi et al. 2013, Kimball et al. 2014).

The global L4_C algorithm error budget for NEE derived during the mission prelaunch phase indicated that the estimated NEE ubRMSE uncertainty is proportional to GPP and is therefore larger in higher biomass productivity areas, including forests and croplands (Kimball et al. 2014). Likewise, NEE ubRMSE uncertainty is expected to be lower in less-productive areas, including grasslands and shrublands. Expected model NEE ubRMSE levels were also generally within targeted accuracy levels for characteristically less-productive boreal and Arctic biomes, even though relative model error as a proportion of total productivity (NEE RMSE / GPP) may be large in these areas. The estimated NEE uncertainty was lower than expected in some warmer tropical high biomass productivity areas (e.g. Amazon rainforest) because of reduced low temperature and moisture constraints to the L4_C respiration calculations so that the bulk of model uncertainty is contributed by GPP in these areas. Model NEE uncertainty in the African Congo was estimated to

be relatively larger than in Amazonia due to relatively drier climate conditions in central Africa and associated larger uncertainty contributions of soil moisture and temperature inputs to the model respiration and GPP calculations.

Detailed global L4_C product assessments and validation activities conducted during the SMAP post-launch Cal/Val and extended mission phases have confirmed that the operational product accuracy and performance is consistent with SMAP L4_C science requirements and product design specifications (e.g., Jones et al. 2017). The latest v5 product release is expected to show consistent or better performance over earlier product versions (v4 or earlier) in relation to independent observational benchmarks; the v5 record is also expected to show no anomalous artifacts or inconsistencies over the extended operational record.

3 V5 PRODUCT UPDATES FROM PRIOR V4 RELEASE

The latest SMAP L4_C v5 product includes the following updates that differ from the prior v4 product release:

- L4_C daily processing uses SMAP operational L4_SM v5 soil moisture inputs from the latest evolution of the SMAP GEOS land model assimilation system (i.e., based on land model version NRv8.3 for v5 vs NRv7.2 for v4);
- Recalibrated L4_C model Biome Properties Lookup Table (BPLUT) and re-initialized model surface soil organic carbon (SOC) pools using MODIS Collection 6 fPAR, MERRA-2 reanalysis daily surface meteorology, and SMAP Nature Run (NRv8.3) L4_SM daily soil moisture and soil temperature inputs;
- BPLUT recalibration using tower eddy covariance CO_2 flux records from 329 sites covering all major global plant functional type (PFT) classes represented in the La Thuile and FLUXNET2015 tower synthesis records;
- Spatially re-weighted BPLUT calibration emphasizing northern (≥45˚N) tower sites and boreal-Arctic biomes;
- Implementation of more stringent bounds on PFT-specific parameters during the BPLUT recalibration for improved realism and consistency with prior literature;
- Other minor adjustments, including updates to product bitflag attribute descriptions and metadata; and updates to HDF5 file format version compatibility (v.1.8 to v.1.10);
- All changes were limited to model inputs, ancillary files and post-processing, with no changes to the core algorithms.

4 ASSESSMENTS

4.1 Global V5 differences from prior product release (V4)

General global patterns and seasonal dynamics of the major L4_C land parameters were evaluated in the latest (v5) product to confirm that the model outputs capture characteristic global environmental patterns and seasonality and show general consistency with the previous (v4) L4_C operational record. These qualitative assessments were also used to identify any potential model errors or anomalies requiring more detailed error diagnostics. The L4_C model processing is conducted at a daily time step and 1-km spatial resolution consistent with MODIS fPAR and land cover (PFT) inputs. The L4_C product outputs are posted to a 9-km resolution global EASE-grid

(version 2), consistent with that of the SMAP Level 4 daily soil moisture (L4_SM) inputs. Primary L4_C product fields include gross primary production (GPP) and soil heterotrophic respiration (RH), which together determine NEE. The L4_C daily product fields also include surface (top 5 cm depth) SOC, derived as the difference between estimated soil litterfall inputs from GPP and respired carbon (CO_2) losses from soil litter decomposition and RH.

A comparison of estimated multi-year (2016-2019) mean annual GPP global patterns from the v5 (Vv5040) and v4 (Vv4040) L4_C products is shown in **Figure 1**. The v5 record captures the characteristic global and seasonal patterns in ecosystem productivity and is largely consistent with the earlier (v4) product release. GPP is generally most productive over the wet tropics and lowest over arid climate regions owing to stronger moisture constraints to productivity. The seasonal variation in GPP is also larger over the high latitudes relative to the tropics, consistent with the general reduction in the annual growing season at higher latitudes. While the v5 and v4 records are largely consistent in terms of GPP distributions, the v5 record indicates slightly less productivity overall due to an overall reduction of the light-use efficiency (LUE) parameters for each BPLUT, in line with recent studies on the global variation in LUE (Madani et al. 2017).

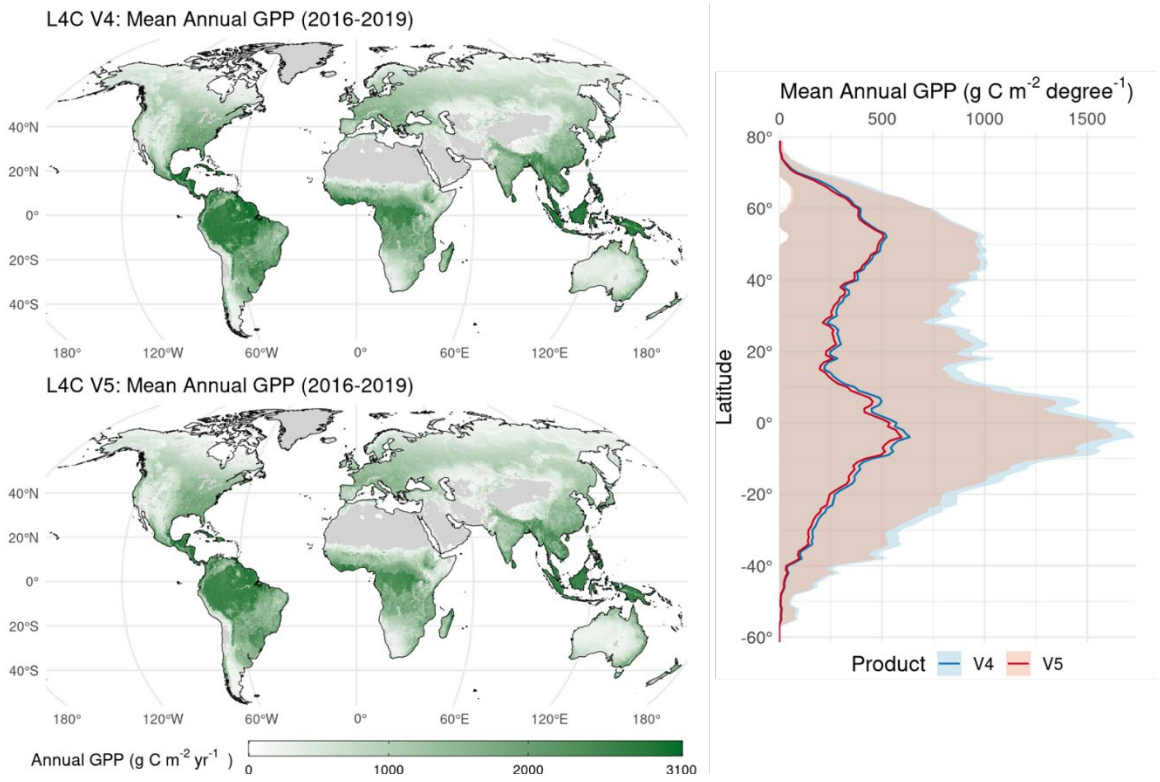

Figure 1. Global patterns of mean annual (2016-2019) GPP (g C m^{-2} yr^{-1}) extracted from the SMAP L4_C v4 and v5 data records (left), and the GPP spatial averages within 1-degree latitude bins (right). Shading in the plot on the right denotes 1 spatial standard deviation within each GPP latitude bin for the v4 and v5 products. Both product versions show consistency in representing characteristic spatial and seasonal patterns and magnitudes in global ecosystem productivity.

A similar global comparison of the estimated multi-year (2016-2019) mean annual soil heterotrophic respiration (RH) pattern from the L4_C v5 and v4 products is depicted in **Figure 2**. The RH pattern is generally proportional to GPP due to the dependence of soil litter decomposition and SOC on GPP litterfall inputs and to similar soil moisture and temperature-related controls on

photosynthesis and respiration. Both v5 and v4 records show strong consistency in depicting the characteristic global RH patterns and seasonality. RH is generally higher in the wet tropics where GPP is largest and soil temperature and moisture conditions are optimal for SOC decomposition. RH rates are lowest in sparsely vegetated cold and arid climates due to increasing cold temperature and soil moisture-related constraints on soil decomposition, as well as to relatively low SOC accumulation due to minimal productivity. In other climate zones (e.g. boreal-Arctic, temperate and semi-arid regions), RH shows larger characteristic seasonality due to larger seasonal variations in moisture and cold temperature constraints. RH is slightly lower in v5 relative to v4 due to the aforementioned reduction in GPP and to the changed surface soil moisture parameters, which create a stronger response to soil moisture deficits but an attenuated response to higher soil moisture conditions.

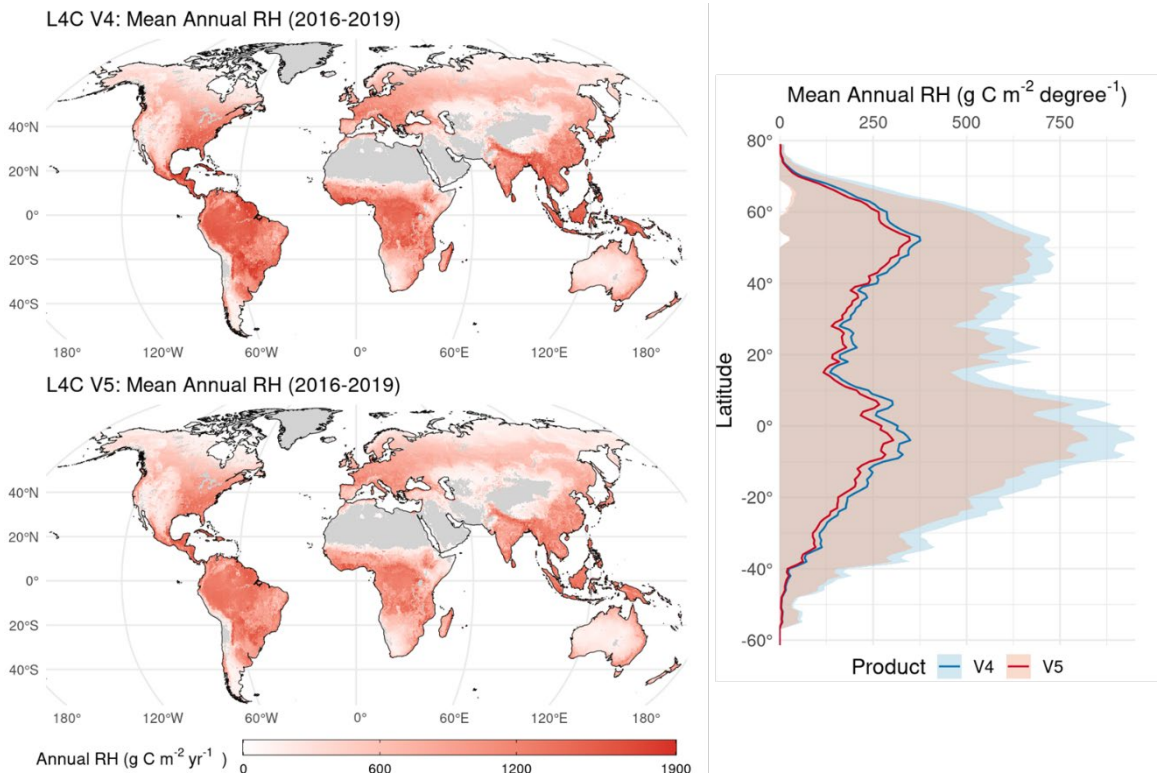

Figure 2. Global patterns of mean annual (2016-2019) RH (g C m^{-2} yr^{-1}) extracted from the SMAP L4_C v4 and v5 data records (left), and the RH spatial averages within 1-degree latitude bins (right). Shading in the plot on the right denotes 1 spatial standard deviation of RH within each latitude bin for the v4 and v5 products. Both product versions show consistency in representing characteristic spatial and seasonal patterns and magnitudes in soil respiration, which are roughly proportional to GPP and accumulated SOC pools.

A comparison of estimated mean annual (2016-2019) SOC stocks from the L4_C v5 and v4 product releases is presented in **Figure 3**. The L4_C v5 and v4 releases both capture expected characteristic patterns and seasonality of global surface SOC. For example, both indicate higher SOC stocks in cold, northern boreal forest and tundra biomes, which are estimated to hold more than half of the global soil carbon. The L4_C SOC map also shows relatively high soil carbon storage in temperate forest areas due to high forest productivity rates and cool, moist soils that promote soil carbon storage. Lower SOC levels occur over dry climate zones, including desert areas in the southwest USA, congruent with generally low productivity levels, warm climate conditions and associated low SOC accumulations. However, SOC levels are elevated in some semi-arid regions, in contrast with relatively low annual productivity; this is due to strong seasonal

soil moisture and temperature restrictions to soil decomposition, which promote SOC accumulation (Endsley et al. 2020). The L4_C results also show relatively low SOC levels in the wet tropics; here, high characteristic GPP and associated litterfall rates are offset by optimal conditions for rapid SOC decomposition and RH emissions, so that most terrestrial carbon storage in the tropics is in vegetation biomass (Baccini et al. 2012).

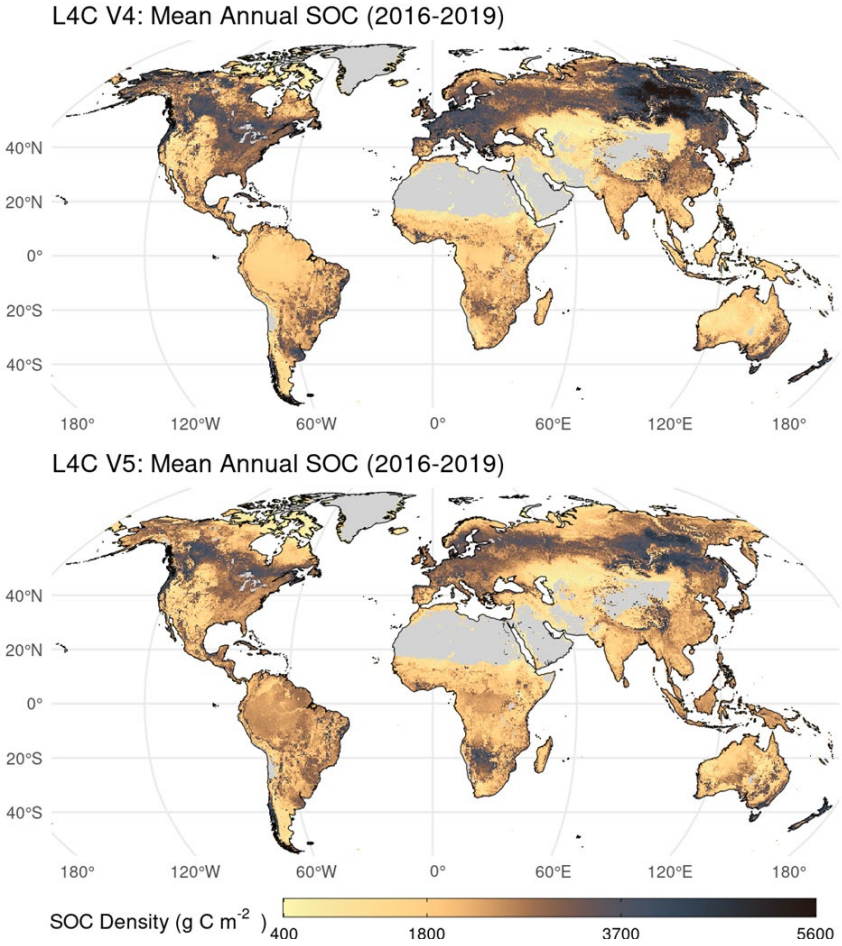

Figure 3. Estimated mean annual (2016-2019) surface (~ top 5 cm) SOC (g C m^{-2}) from the SMAP L4_C v5 operational record in relation to the previous v4 release. The SOC estimates are derived at a 1-km spatial resolution during L4_C processing and posted to a 9-km resolution spatial grid. Grey shading denotes barren land, permanent ice, open water and other areas outside of the model domain. A summary of SOC stocks by latitude band is shown in Figure 10 in Section 4.3.3.

4.2 Performance against Tower Core Validation Sites

The L4_C derived daily carbon fluxes for NEE, GPP and ecosystem respiration (RECO; derived as the daily sum of RH and autotrophic respiration) from the latest v5 product release were compared against in situ daily tower eddy covariance carbon flux observations from 26 L4_C core validation tower sites (CVS) over the available three-year (2015-2017) CVS record. The v5 performance was also assessed in relation to the L4_C v4 record and the latest L4_C Nature Run (NRv8.3). The NRv8.3 record is derived without the direct influence of assimilated SMAP brightness temperatures in the GEOS system. Differences in L4_C accuracy among the three product sets (NRv8.3, v5, and v4) relative to the independent CVS observational benchmark

provides a measure of potential v5 accuracy gains relative to the earlier (v4) product release (v5 compared to v4), and the impact of the SMAP operational data assimilation on product performance (v5 compared to NRv8.3). Primary metrics used for the CVS comparisons included Pearson correlation and root mean squared error (RMSE) differences between L4_C estimated and tower-observed daily carbon fluxes.

Unlike the historical FLUXNET tower eddy covariance records used for the model BPLUT calibration, the CVS observations are independent of the L4_C model and overlap with the SMAP operational record. The SMAP L4_C CVS sites are summarized in **Table 1**, while the CVS locations are presented in **Figure 4** along with the larger set of FLUXNET (La Thuile and FLUXNET2015) tower sites used for the L4_C BPLUT calibration (Jones et al. 2017).

Table 1. CVS sparse tower network used for intensive L4_C product assessments.

[1]Site	[2]PFT	Lat	Lon	Location	Full Name
FI-Sod	ENF	67.36	26.64	Finland	FMI Sodankyla
CA-Oas	ENF	53.99	-105.12	Sask. CN	BERMS Southern Old Black Spruce
US-ICt	SHR	68.61	-149.30	AK, USA	Imnavait Tussock
US-ICh	SHR	68.61	-149.30	AK, USA	Imnavait Heath
US-ICs	SHR	68.61	-149.31	AK, USA	Imnavait Wet Sedge
US-BZs	ENF	64.70	-148.32	AK, USA	Bonanza Creek Black Spruce
US-BZb	ENF	64.70	-148.32	AK, USA	Bonanza Creek Bog
US-BZf	ENF	64.70	-148.31	AK, USA	Bonanza Creek Fen
US-PFa	DBF	45.95	-90.27	WI, USA	Park Falls
US-Atq	GRS	70.47	-157.41	AK, USA	Atqasuk
US-Ivo	SHR	68.49	-155.75	AK, USA	Ivotuk
US-SRM	SHR	31.82	-110.87	AZ, USA	Santa Rita Mesquite
US-Wkg	GRS	31.74	-109.94	AZ, USA	Walnut Gulch Kendall Grasslands
US-Whs	SHR	31.74	-110.05	AZ, USA	Walnut Gulch Lucky Hills Shrubland
US-Ton	SHR	38.43	-120.97	CA, USA	Tonzi Ranch
US-Var	SHR	38.41	-120.95	CA, USA	Vaira Ranch
AU-Whr	SHR	-36.67	145.03	Australia	Whroo
AU-Rig	CRP	-36.66	145.58	Australia	Riggs Creek
AU-Ync	CRP	-34.99	146.29	Australia	Yanco
AU-Stp	GRS	-17.15	133.35	Australia	Sturt Plains
AU-Dry	GRS	-15.26	132.37	Australia	Dry River
AU-DaS	GRS	-14.16	131.39	Australia	Daily River Savannah
AU-How	GRS	-12.50	131.15	Australia	Howard Springs
AU-GWW	SHR	-30.19	120.65	Australia	Great Western Woodlands
AU-ASM	SHR	-22.28	133.25	Australia	Alice Springs
AU-TTE	SHR	-22.29	133.64	Australia	Ti Tree East

[1]FLUXNET based tower site identifiers; [2]Tower PFT classes defined from a 1-km resolution MODIS (MOD12Q1) Type 5 (8 vegetation class) global land cover map, consistent with L4_C processing.

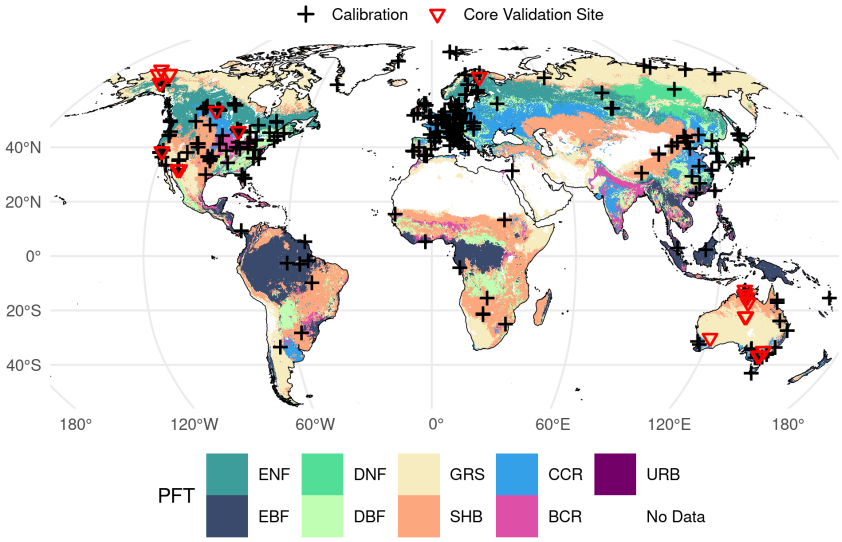

Figure 4. Locations of the core tower validation sites (CVS) used for the L4_C product assessment. FLUXNET sites with historical tower records used for the L4_C model BPLUT calibration are also shown in relation to global plant functional types summarized from the MODIS MOD12Q1 (8 vegetation class) global land cover classification (Friedl et al. 2010).

The mean correlations and RMSEs between the CVS observations and L4_C outputs for the daily carbon fluxes (NEE, GPP and RECO) are shown in **Figure 5**. The three-year (2015-2017) period for the comparisons is defined by the availability of the 26 CVS tower site records. The results show the relative differences in L4_C performance between the latest v5 operational product release, the previous v4 release, and the v5 Nature Run (NRv8.3). The results show clear improvement in v5 performance over the v4 and NRv8.3 records for NEE, indicated by higher correlations and lower RMSEs relative to the independent global CVS network observations. Both L4_C operational products (v5 and v4) show better performance than the v5 Nature Run (NRv8.3) for NEE, indicating a clear benefit of the SMAP observations on L4_C accuracy. The v5 NEE results also remain well within the targeted L4_C performance threshold (mean NEE RMSE $\leq$ 1.6 g C m^{-2} d^{-1}).

The L4_C v5 performance gain is smaller for the other carbon fluxes (GPP and RECO). The v5 performance for GPP and RECO is largely consistent with or slightly better than the v4 product based on the mean correlations and RMSEs. However, both v5 and v4 show very similar or only slightly better performance than the L4_C Nature Run. Thus, while the latest v5 operational release shows clear performance improvement in the targeted NEE variable, the component carbon fluxes for GPP and RECO remain largely consistent with the prior v4 release based on the global CVS site comparisons. The favorable performance of the NRv8.3 results also show that the L4_C carbon model and GEOS land model assimilation framework are capable of producing science quality data, even without the direct benefit of SMAP observations.

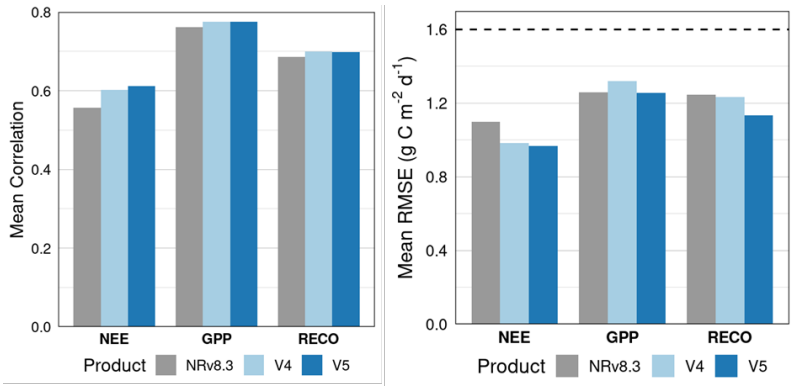

Figure 5. Summary of global CVS site comparisons between daily tower observations and L4_C daily product outputs for NEE, GPP and RECO over the available three years of continuous daily tower observations (2015-2017); reported metrics include mean correlations and RMSE across all sites. L4_C outputs include the latest v5 operational product, the previous v4 product, and the latest v5 model Nature Run (NRv8.3). The targeted daily NEE RMSE threshold for the L4_C product (1.6 g C m^{-2} d^{-1}) is denoted by the horizontal dashed line in the right panel.

4.3 Consistency with Other Global Carbon Products

The L4_C product outputs were compared against similar variables from other available global carbon products. The objective of these comparisons was to assess and document the general consistency of selected L4_C operational product fields compared to similar variables from other global benchmark datasets commonly used by the community. These benchmark datasets incorporate some independent information and utilize different statistical techniques to derive estimates of global carbon fluxes and SOC state. The global data products examined include:

1) FLUXNET machine-learning upscaled global carbon fluxes from the FLUXCOM initiative using the remote sensing plus meteorological/climate forcing (RS+METEO) setup (Jung et al. 2020);
2) Solar-Induced canopy Fluorescence (SIF) observations from the ESA GOME-2 (Global Ozone Mapping Experiment) satellite sensor (Joiner et al. 2013);
3) Global SOC records from the SoilGrids-250 m machine learning-based soil inventory extrapolation (Hengl et al. 2017);
4) TRENDYv7 ensemble simulations from dynamic global vegetation models (DGVMs; Le Quéré et al. 2018).

The global comparisons spanned at least three complete annual cycles (2016-2018) within the SMAP operational record. The period used for evaluation was also distinct from that of the BPLUT calibration (section 4.2). The FLUXCOM data provide continuous global daily extrapolations of NEE and GPP that extend well beyond the limited tower eddy covariance sampling footprints represented from the CVS comparison, while effectively integrating the extensive FLUXNET global tower observational record with other synergistic remote sensing and surface meteorological information within an ensemble machine learning model extrapolation framework; these data were used to verify regional patterns, seasonal behavior, and interannual variability in the L4_C carbon flux record. The composited monthly SIF record from GOME-2 was also used as an observational proxy for GPP (Madani et al. 2017) and provided an additional check on global patterns and seasonal-to-interannual variability in L4_C GPP. The SoilGrids and TRENDYv7 DGVM ensemble global SOC records were also used to verify the relative magnitude and global

distribution of the L4_C derived surface SOC outputs. The detailed summaries of these comparisons are provided in the following sub-sections.

4.3.1 FLUXCOM

The L4_C mean daily NEE and GPP were compared against similar FLUXCOM carbon flux extrapolations for the overlapping three-year record (2016-2018). The FLUXCOM record used for this comparison is derived using an ensemble of three machine learning methods and five global climate forcing datasets for empirical upscaling of tower-based daily carbon flux observations from the global FLUXNET data archive (Jung et al. 2020). The spatial upscaling approach also uses other explanatory geospatial variables from mean seasonal cycles of satellite data and daily meteorology observations (RS+METEO). The FLUXCOM data are available on a 0.5-degree resolution global grid, whereas the L4_C product is produced in a finer 9-km resolution global EASE-grid v2 format. For the comparison, the L4_C and FLUXCOM data were spatially aggregated and compared over a consistent set of global TransCom subregions (Gurney et al., 2004).

The seasonal and annual variation in NEE and GPP for the major TransCom regions indicated from the L4_C and FLUXCOM records are presented in **Figure 6**. Grey shading in the figure denotes approximate 95% confidence intervals for the FLUXCOM mean values within each subregion. Both L4_C v5 and v4 records are also shown to evaluate potential differences in product versions relative to the FLUXCOM benchmark. Overall, the results show strong consistency between the L4_C v5 and v4 products across all global sub-regions and over the multi-year operational record. The L4_C results also show favorable correspondence with the FLUXCOM record in capturing the regional magnitudes and multi-year seasonal cycles in both NEE (median r=0.78, RMSE<1.33 g C m^{-2} d^{-1}) and GPP (median r=0.96, RMSE<0.93 g C m^{-2} d^{-1}, excluding the South American Tropical region). The relative agreement between L4_C and FLUXCOM derived carbon fluxes is generally within the range of uncertainty for FLUXCOM spatial means (in grey). The relative agreement is also stronger for GPP due to NEE being a residual difference of two larger carbon fluxes (GPP and RECO). While the L4_C and FLUXCOM results show generally favorable correspondence, some systematic regional differences are apparent. For example, the L4_C results show less NEE carbon sink strength over the tropics due to a larger L4_C respiration flux relative to FLUXCOM. Similarly, in regions that have both strong sinks and sources co-occurring in the same season, as in Australia and the South American Tropics (evident in the FLUXCOM confidence bands), the spatial means show less correspondence due to low characteristic variability near the equator.

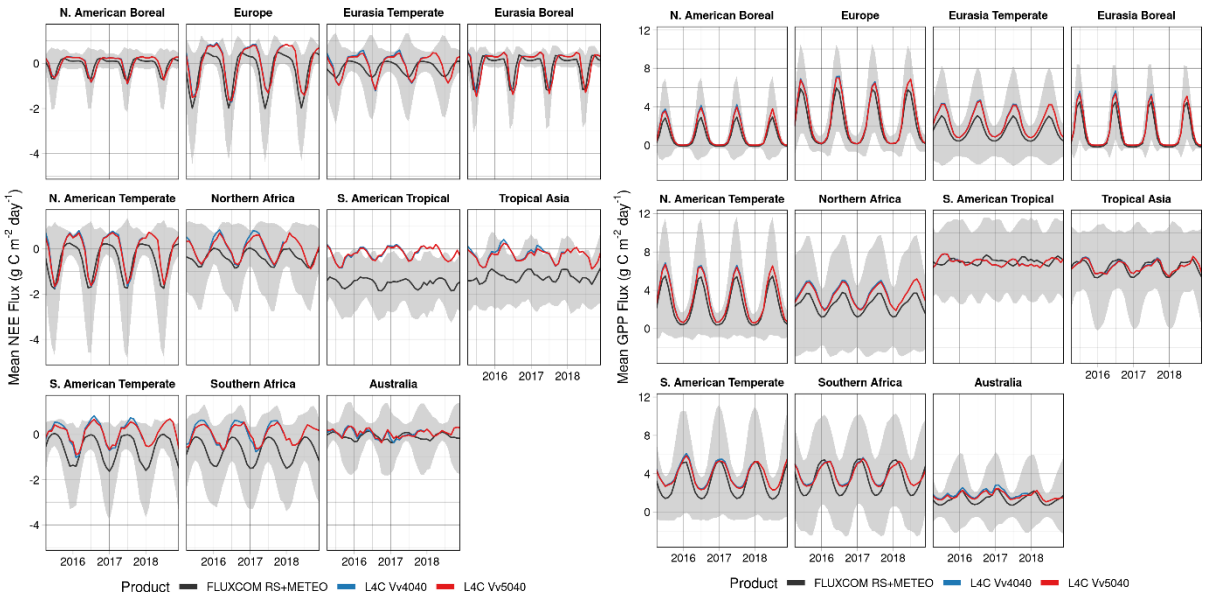

Figure 6. Comparison of mean daily NEE and GPP outputs from the SMAP L4_C and FLUXCOM global data products aggregated over the Transcom global subregions. The FLUXCOM mean daily carbon fluxes are shown by the black line, while the 95% confidence bands of the FLUXCOM GPP and NEE spatial means within each sub-region are shown by the grey shading. The L4_C mean daily outputs from the current v5 (Vv5040) and prior v4 (Vv4040) product releases are shown by the red and blue lines, respectively.

4.3.2 GOME-2 SIF

The global patterns in mean annual productivity indicated from the L4_C v5 GPP and GOME-2 SIF records are shown in **Figure 7**. The SIF data from the ESA GOME-2 sensor are available as composited monthly means at a 0.5-degree spatial resolution in geographic projection. The SIF data were therefore re-projected to the same 9-km resolution global EASE-Grid (v2) format of the L4_C product using nearest-neighbor resampling. Since SIF is a byproduct of plant photosynthesis, the data are normalized to account for global variations in photosynthetically active radiation (PAR). SIF (mW m^{-2} sr^{-1} nm^{-1}) is proportional to GPP (g C m^{-2} d^{-1}), but the relationship can vary according to PFT and environmental conditions (Porcar-Castell et al. 2014). However, both the GOME-2 SIF and L4_C GPP results show a similar global pattern of annual productivity. Both products show the greatest productivity in wet tropical forests and lowest productivity in the polar climate and arid desert regions. Both products also show similar intermediate levels of productivity in temperate forests and agricultural regions. The L4_C annual productivity pattern is relatively smooth compared to the SIF record because the GOME-2 observations are subject to greater background noise and data loss from low solar illumination and atmospheric contamination effects than is the model based L4_C product, particularly at high latitudes.

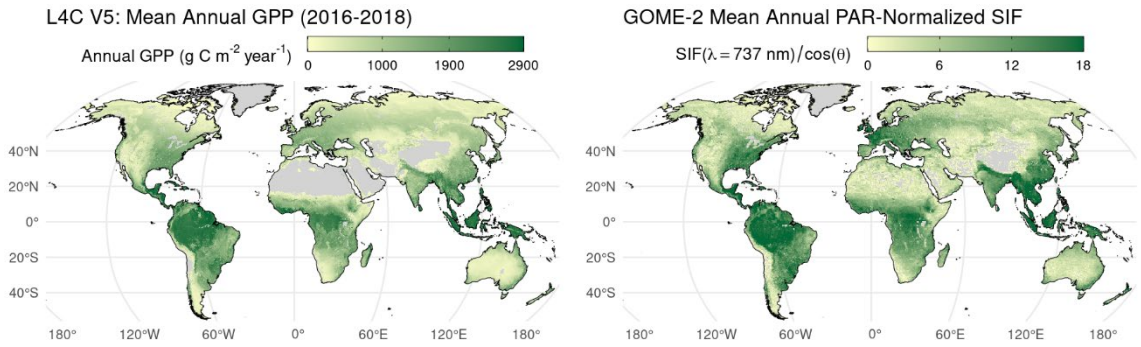

Figure 7. Comparison of global mean annual productivity patterns indicated from the SMAP L4_C v5 GPP and GOME-2 PAR-normalized SIF record for the 2015-2018 overlapping record.

The mean r^2 correspondence in global monthly productivity (2016-2018) between the L4_C v5 GPP and GOME-2 SIF records is shown in **Figure 8**. Here, we compared two linear models: one in which L4C GPP has a simple linear relationship with GOME-2 SIF (blue line) and one in which that relationship varies by PFT (red line); the horizontal bars show the spread (minimum to maximum) in monthly r^2 values across the years. Overall, GOME-2 SIF explains between 62 and 83 percent of the variance in monthly L4_C v5 GPP. The correspondence is lower during the Northern Hemisphere winter months due to the larger area of seasonal darkness and winter dormancy over the higher latitudes; the larger area of winter snow cover and reduced solar illumination at higher latitudes also contributes to greater data loss in the GOME-2 SIF record. In contrast, the global GPP and SIF records show the strongest agreement from August to September (r^2~80%).

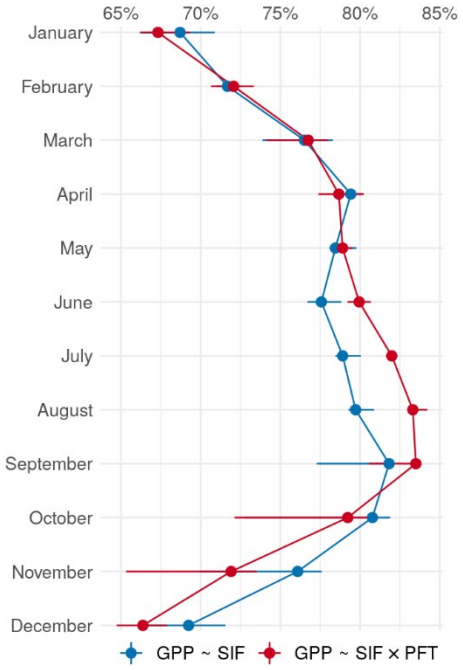

Figure 8. Mean Coefficient of Determination (r^2) between L4_C v5 GPP and GOME-2 SIF composited monthly records. The GPP record is aggregated from L4_C daily outputs and regressed spatially against PAR-normalized SIF during each year of 2016-2018. The goodness-of-fit (r^2) is shown for a simple linear relationship (blue) and for a linear relationship where the slope varies by PFT (red); horizontal lines denote the spread (minimum to maximum over the three years) in the monthly spatial r^2 over the global domain.

Standardized monthly anomalies (Z-scores) in L4_C v5 (Vv5040) and v4 (Vv4040) GPP compare well against the GOME-2 SIF record in most regions, particularly in Australia and in North America (**Figure 9**). Anomalies in both L4C GPP and GOME-2 SIF correspond in part with the ENSO phase, as measured by the El Niño outgoing long-wave radiation (OLR) event index (Chiodi and Harrison 2013). Large variations in GPP and SIF anomalies in 2015-2016 correspond with strong swings in the OLR event index during that recent record El Niño year (not shown), as evident in the subplots for the South American Temperate and North American Boreal regions (Figure 9). The L4_C v5 productivity anomalies are largely consistent with the prior v4 GPP record over all Transcom subregions. However, the short period of overlap between the L4_C and GOME-2 SIF records limits the generalization of this finding.

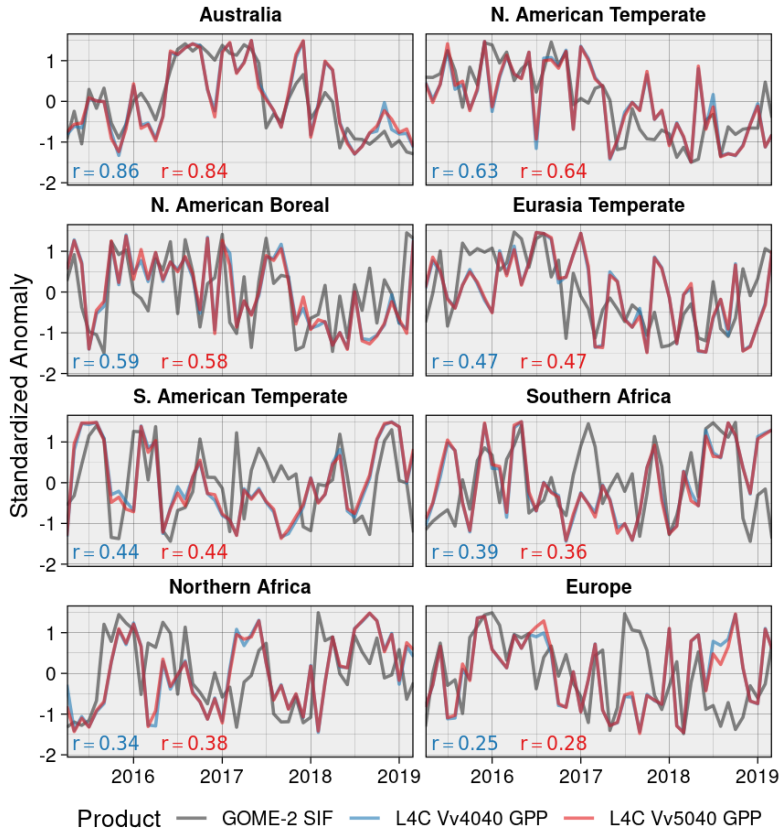

Figure 9. Standardized monthly anomalies (Z-scores) for L4_C GPP and GOME-2 SIF are plotted for the period March 2015 – March 2019 for each TransCom region. Pearson's correlations between the L4_C GPP version 4 (blue) and version 5 (red) time series and the SIF record are displayed at the bottom left of each subplot.

4.3.3 SOC Records

The L4_C surface SOC product is an estimate of the SOC content in the surface (0-5 cm) soil layer. The long-term mean, global SOC density map for 2016-2018 was scaled to SOC storage and summarized by latitude band in **Figure 10** for comparison with other global SOC inventories, after Endsley et al. (2020). The latitudinal pattern of SOC revealed in this summary compares well to the data-driven SoilGrids 250m product, as well as to the TRENDYv7 ensemble mean (Figure 10). The pattern compares most favorably at high northern latitudes, where L4_C SOC appears to slightly underestimate SOC storage (likely due to unaccounted-for deep SOC in boreal and arctic soils) but is well within +/- 1 standard deviation of the TRENDYv7 ensemble mean. L4_C shows

relatively larger SOC storage in the southern extra-tropics (below 20 degrees S latitude) and also somewhat greater storage in the tropics. The larger L4_C SOC levels in these southern hemisphere areas may reflect greater uncertainty in the SoilGrids and TRENDYv7 datasets due to relatively sparse ground truth compared to the northern hemisphere; however further L4_C refinements in these areas may be targeted in future re-processing events.

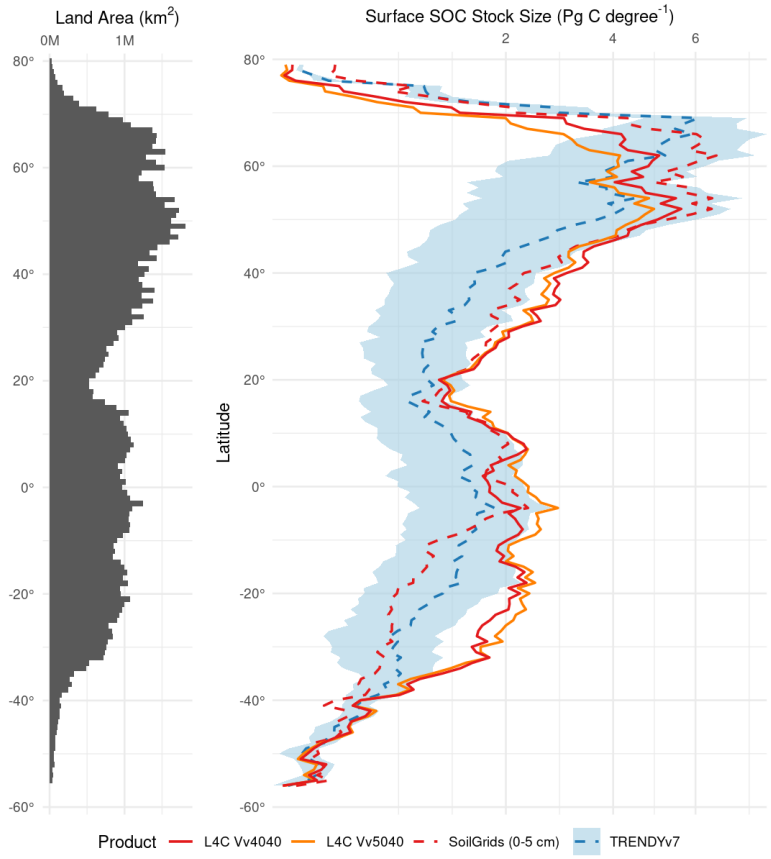

Figure 10. Global distribution of surface (0-5cm) SOC estimates from multiple datasets, spatially averaged by 1-degree latitudinal bins; the total land area represented within each latitudinal bin is also shown (left). The SOC records depicted include the L4_C v5 (Vv5040) and v4 (Vv4040) products; SoilGrids; and the TRENDYv7 DGVM ensemble mean. Datasets shown with a dotted line are interpolated to a 5-cm surface soil layer consistent with the L4_C SOC product. The TRENDYv7 ensemble mean is shown as a line, while the shaded area corresponds to ±1 standard deviation in the associated DGVM predictions.

4.4 Summary

This report provides an assessment of the latest (v5) SMAP Level 4 Carbon (L4_C) product release. Methods used to ascertain the v5 product quality and performance relative to the prior (v4) L4_C release involved a multi-year operational record and: 1) qualitative evaluations of the degree to which selected product fields represent characteristic global patterns and magnitudes in terrestrial carbon fluxes and surface SOC stocks; 2) comparisons of daily product outputs with tower eddy covariance measurement-based daily carbon (CO_2) flux observations from a global network of core (CVS) tower sites; 3) consistency checks of L4_C product fields against other synergistic global carbon products, including FLUXCOM, GOME-2 SIF, soil inventory and DGVM-based SOC records.

Based on these assessments, the L4_C v5 product demonstrates a level of performance and accuracy consistent with the algorithm and product design. The L4_C v5 product shows expected characteristic global patterns and seasonality in estimated carbon fluxes and SOC stocks, with no apparent artifacts or errors in algorithm performance or formatting. The global performance assessment indicates that the L4_C v5 product is well within the targeted accuracy requirements for NEE (mean RMSE $\leq$ 1.6 g C m^{-2} d^{-1}) and shows consistent or improved performance over the prior (v4) release based on the CVS network tower comparisons. The major L4_C product fields are also generally consistent with similar variables obtained from a diverse set of global benchmark environmental data records. The latest L4_C v5 product replaces previous (v4 and earlier) product versions and continues to show favorable accuracy and consistent performance over a multi-year record that meet or exceed SMAP L4_C science requirements. Therefore, the L4_C product continues to be well suited for a diversity of science applications as demonstrated from previous studies, including global assessments of ecosystem productivity and terrestrial carbon sink activity, agricultural assessments of crop conditions and annual crop yields, and assessments of regional drought impacts and environmental drivers.

5 POTENTIAL FUTURE L4_C PRODUCT UPDATES

Future releases of the SMAP L4_C operational product are expected to incorporate ongoing Cal/Val refinements and improvements in the SMAP brightness temperature observations and the GEOS land model assimilation system, along with potential updates to other L4_C inputs. Future product releases may also incorporate refinements and potential improvements to the L4_C Terrestrial Carbon Flux (TCF) model. Potentially significant updates may include:

- *Improvements to the GEOS assimilation system.* The NASA GEOS system provides the SMAP L4_SM daily surface and root soil moisture and soil temperature inputs required for L4_C production. The system undergoes periodic refinements and updates to the land model, assimilation, and observational inputs that may contribute to improvements in the L4_SM and L4_C products. These improvements will be accounted for in future product releases, through L4_C recalibration and re-initialization procedures.
- *Transition from MODIS to VIIRS as primary source for fPAR inputs.* The L4_C operations require global operational fPAR 8-day time series as primary inputs to define vegetation photosynthetic canopy cover and phenology for estimating GPP. The current baseline for the fPAR inputs is the MODIS 8-day 500m MOD15A2H (C6) record. However, the MODIS sensors on both NASA EOS Terra and Aqua satellites are nearing end-of-mission. Potential loss of MODIS fPAR inputs will require a shift to another alternative fPAR source to maintain optimal L4_C operations. Planning is underway to shift L4_C preprocessing to use the JPSS/NPP VIIRS 8-day global 500m fPAR operational record (VNP15A2H), which will become the baseline for future L4_C operations and product releases.
- *Improvements to TCF model respiration phenology.* Planning is underway to evaluate potential improvements in model NPP litterfall allocation and autotrophic respiration phenology gained from recent science advances. More realistic representations of these factors could potentially improve estimated seasonality in RECO and NEE.

6 ACKNOWLEDGEMENTS

Funding for this work was provided by the SMAP mission. Computing resources were provided by the NASA Center for Climate Simulation. This work used eddy covariance data acquired by the FLUXNET community, which was supported by the CarboEuropeIP, CSIRO, FAO-GTOS-TCO, iLEAPS, Max Planck Institute for Biogeochemistry, National Science Foundation, National Research Insfrastructure for Australia, Terrestrial Ecosystem Research Network, University of Tuscia, Université Laval and Environment Canada, US Department of Energy and NOAA ESRL, as well as many local funders including the Global Change Research Centre AS Czech Republic, Wisconsin Focus on Energy, and Forest Department of the Autonomous Province of Bolzano – CO_2-measuring station of Renon/Ritten. We thank Drs. A.E. Andrews, M. Aurela, D. Baldocchi, J. Beringer, P. Bolstad, J. Cleverly, B.D. Cook, K.J. Davis, A.R. Desai, D. Eamus, E. Euskirchen, J. Goodrich, L. Hutley, A. Kalhori, H. Kwon, B. Law, C. Macfarlane, W. Oechel, S. Prober, K. Rautiainen, R. Scott, H. Wheater, D. Zona and many other PIs for sharing their flux tower data.

7 REFERENCES

Baccini, A., S.J. Goetz, W.S. Walker, et al., 2012. Estimated carbon dioxide emissions from tropical deforestation improved by carbon-density maps. *Nature Climate Change*, **2**, 182-185.

Baldocchi, D., 2008: Breathing of the terrestrial biosphere: lessons learned from a global network of carbon dioxide flux measurement systems. *Austr. J. Bot.*, **56**: 1-26.

Chiodi, A. M., & Harrison, D. E. (2013). El Niño impacts on seasonal U.S. atmospheric circulation, temperature, and precipitation anomalies: The OLR-Event perspective. *Journal of Climate*, **26**(3), 822–837.

Endsley, K.A., J.S. Kimball, R.H. Reichle, and J.D. Watts, 2020. Satellite monitoring of global surface soil organic carbon dynamics using the SMAP Level 4 Carbon product. *JGR Biogeosciences* **125**(12), e2020JG006100, https://doi.org/10.1029/2020JG006100.

Entekhabi, D., E.G. Njoku, P.E. O'Neill, et al., 2010. The Soil Moisture Active and Passive (SMAP) Mission. *Proceedings of the IEEE* **98**(5), 704-716.

Entekhabi, D., S. Yueh, P. O'Neill, K. Kellogg et al., SMAP Handbook, JPL Publication, JPL 400-1567, Jet Propulsion Laboratory, Pasadena, California, 182 pages, 2014. https://smap.jpl.nasa.gov/files/smap2/SMAP_Handbook_FINAL_1_JULY_2014_Web.pdf.

Friedl, M.A., D. Sulla-Menashe, B. Tan, A. Schneider, N. Ramankutty, A. Sibley, and X. Huang, 2010. MODIS Collection 5 global land cover: Algorithm refinements and characterization of new datasets. *Remote Sensing of Environment* **114**(1), 168-182.

Glassy, J., J.S. Kimball, R.H. Reichle, J.V. Ardizzone, G-K. Kim, R.A. Lucchesi, and B.H. Weiss, 2015. Soil Moisture Active Passive (SMAP) Mission Level 4 Carbon (L4_C) Product Specification Document. GMAO Office Note No. 12 (Version 1.9), 71 pp, NASA Goddard Space Flight Center, Greenbelt, MD, USA. Available from http://gmao.gsfc.nasa.gov/pubs/office_notes.

Hengl, T., J. M. de Jesus, G.B.M. Heuvelink, et al., 2017. SoilGrids250m: Global gridded soil information based on machine learning. *PLOS ONE*, **12**(2): https://doi.org/10.1371/journal.pone.0169748 .

Jackson, T., A. Colliander, J. Kimball, R. Reichle, W. Crow, D. Entekhabi, P. O'Neill, and E. Njoku, 2014. SMAP Science Data Calibration and Validation Plan. SMAP Project, JPL D-52544, Jet Propulsion Laboratory, Pasadena CA, 96 pp (http://smap.jpl.nasa.gov/files/smap2/CalVal_Plan_120706_pub.pdf).

Joiner, J., L. Gaunter, R. Lindstrot, et al., 2013. Global monitoring of terrestrial chlorophyll fluorescence from moderate-spectral-resolution near-infrared satellite measurements: methodology, simulations, and application to GOME-2. *Atmos. Meas. Tech*., **6**, 2803-2823.

Jones, L.A., J.S. Kimball, R.H. Reichle, N. Madani, J. Glassy, J.V. Ardizzone, A. Colliander, J. Cleverly, A.R. Desai, D. Eamus, E.S. Euskirchen, L. Hutley, C. Macfarlane, and R.L. Scott, 2017. The SMAP Level 4 Carbon product for monitoring ecosystem land-atmosphere CO2 exchange. *IEEE TGARS,* **55**(11), 6517-6532, doi: 10.1109/TGRS.2017.2729343.

Jung, M., C. Schwalm, M. Migliavacca, et al., 2020. Scaling carbon fluxes from eddy covariance sites to globe: synthesis and evaluation of the FLUXCOM approach. *Biogeosciences*, **17**, 1343-1365.

Kimball, J.S., L.A. Jones, J.P. Glassy, and R. Reichle, 2014. SMAP Algorithm Theoretical Basis Document, Release A: L4 Carbon Product. SMAP Project, JPL D-66484, Jet Propulsion Laboratory, Pasadena CA., 76 pp, (http://smap-archive.jpl.nasa.gov/files/smap2/L4_C_RevA.pdf).

Li, X., J. Xiao, J.S. Kimball, R.H. Reichle, R.L. Scott, M.E. Litvak, G. Bohrer, and C. Frankenberg, 2020. Synergistic use of SMAP and OCO-2 data in assessing the responses of ecosystem productivity to the 2018 U.S. drought. *Remote Sensing of Environment*, **251**, 112062, https://doi.org/10.1016/j.rse.2020.112062.

Liu, Z., J.S. Kimball, N. Parazoo, A. Ballantyne, W. Wen, R. Reichle, C. Pan, J. Watts, O. Sonnentag, P. Marsh, M. Hurkuck, M. Helbig, W. Quinton, D. Zona, M. Ueyama, H. Kobayashi, and E. Euskirchen, 2019. Increased high-latitude photosynthetic carbon gain offset by respiration carbon loss during an anomalous warm winter to spring transition. *Global Change Biology*, **26**(2), 682-696, DOI:10.1111/gcb.14863.

Madani, N., J.S. Kimball, and S.W. Running, 2017. Improving global gross primary productivity estimates by computing optimal light use efficiencies using flux tower data. *J. Geophys. Res. Biogeosci*., **122**(11), 2939-2951.

Madani, N., J.S. Kimball, L.A. Jones, N.C. Parazoo, and K. Guan, 2017. Global analysis of bioclimatic controls on ecosystem productivity using satellite observations of solar-induced chlorophyll fluorescence. *Remote Sensing*, **9**, 530.

Porcar-Castell, A., E. Tyystjarvi, J. Atherton, et al., 2014. Linking chlorophyll a fluorescence to photosynthesis for remote sensing applications: mechanisms and challenges. *Journal of Experimental Botany*, **66**(19), doi:101093/jxb/eru191.

Reichle, R.H., Q. Liu, J.V. Ardizzone, W.T. Crow, G.J.M. De Lannoy, J. Dong, J.S. Kimball, and R.D. Koster, 2020. The contributions of gauge-based precipitation and SMAP brightness

temperature observations to the skill of the SMAP Level-4 Soil Moisture product. *J. Hydrometeorology*, **22**(2), DOI:10.1175/JHM-D-20-0217.1.

Reichle, R., Q. Liu, R.D. Koster, J.V. Ardizzone, A. Colliander, W.T. Crow, G. De Lannoy, J.S. Kimball, J. Kolassa, and S.P. Mahanama, 2019. Version 4 of the SMAP Level-4 soil moisture algorithm and data product. *Journal of Advances in Modeling Earth Systems*, **11**(10), doi:10.1029/2019MS001729.

Wurster, P.M., M. Maneta, J.S. Kimball, K.A. Endsley, and S. Begueria, 2020. Monitoring crop status in the continental United States using the SMAP Level 4 Carbon product. *Frontiers in Big Data*, **3**, 597720.

Yi, Y., J.S. Kimball, L.A. Jones, R.H. Reichle, R. Nemani, and H.A. Margolis, 2013. Recent climate and fire disturbance impacts on boreal and arctic ecosystem productivity estimated using a satellite-based terrestrial carbon flux model. *J. Geophys. Res*. *Biogeosci*., **118**, 1-17.

Previous Volumes in This Series

Volume 1 September 1994	*Documentation of the Goddard Earth Observing System (GEOS) general circulation model - Version 1* L.L. Takacs, A. Molod, and T. Wang
Volume 2 October 1994	*Direct solution of the implicit formulation of fourth order horizontal diffusion for gridpoint models on the sphere* Y. Li, S. Moorthi, and J.R. Bates
Volume 3 December 1994	*An efficient thermal infrared radiation parameterization for use in general circulation models* M.-D. Chou and M.J. Suarez
Volume 4 January 1995	*Documentation of the Goddard Earth Observing System (GEOS) Data Assimilation System - Version 1* James Pfaendtner, Stephen Bloom, David Lamich, Michael Seablom, Meta Sienkiewicz, James Stobie, and Arlindo da Silva
Volume 5 April 1995	*Documentation of the Aries-GEOS dynamical core: Version 2* Max J. Suarez and Lawrence L. Takacs
Volume 6 April 1995	*A Multiyear Assimilation with the GEOS-1 System: Overview and Results* Siegfried Schubert, Chung-Kyu Park, Chung-Yu Wu, Wayne Higgins, Yelena Kondratyeva, Andrea Molod, Lawrence Takacs, Michael Seablom, and Richard Rood
Volume 7 September 1995	*Proceedings of the Workshop on the GEOS-1 Five-Year Assimilation* Siegfried D. Schubert and Richard B. Rood
Volume 8 March 1996	*Documentation of the Tangent Linear Model and Its Adjoint of the Adiabatic Version of the NASA GEOS-1 C-Grid GCM: Version 5.2* Weiyu Yang and I. Michael Navon
Volume 9 March 1996	*Energy and Water Balance Calculations in the Mosaic LSM* Randal D. Koster and Max J. Suarez

Volume 10 April 1996	*Dynamical Aspects of Climate Simulations Using the GEOS General Circulation Model* Lawrence L. Takacs and Max J. Suarez
Volume 11 May 1997	*Documentation of the Tangent Linear and Adjoint Models of the Relaxed Arakawa-Schubert Moisture Parameterization Package of the NASA GEOS-1 GCM (Version 5.2)* Weiyu Yang, I. Michael Navon, and Ricardo Todling
Volume 12 August 1997	*Comparison of Satellite Global Rainfall Algorithms* Alfred T.C. Chang and Long S. Chiu
Volume 13 December 1997	*Interannual Variability and Potential Predictability in Reanalysis Products* Wie Ming and Siegfried D. Schubert
Volume 14 August 1998	*A Comparison of GEOS Assimilated Data with FIFE Observations* Michael G. Bosilovich and Siegfried D. Schubert
Volume 15 June 1999	*A Solar Radiation Parameterization for Atmospheric Studies* Ming-Dah Chou and Max J. Suarez
Volume 16 November 1999	*Filtering Techniques on a Stretched Grid General Circulation Model* Lawrence Takacs, William Sawyer, Max J. Suarez, and Michael S. Fox-Rabinowitz
Volume 17 July 2000	*Atlas of Seasonal Means Simulated by the NSIPP-1 Atmospheric GCM* Julio T. Bacmeister, Philip J. Pegion, Siegfried D. Schubert, and Max J. Suarez
Volume 18 December 2000	*An Assessment of the Predictability of Northern Winter Seasonal Means with the NSIPP1 AGCM* Philip J. Pegion, Siegfried D. Schubert, and Max J. Suarez
Volume 19 July 2001	*A Thermal Infrared Radiation Parameterization for Atmospheric Studies* Ming-Dah Chou, Max J. Suarez, Xin-Zhong Liang, and Michael M.-H. Yan

Volume 20 August 2001	*The Climate of the FVCCM-3 Model* Yehui Chang, Siegfried D. Schubert, Shian-Jiann Lin, Sharon Nebuda, and Bo-Wen Shen
Volume 21 September 2001	*Design and Implementation of a Parallel Multivariate Ensemble Kalman Filter for the Poseidon Ocean General Circulation Model* Christian L. Keppenne and Michele M. Rienecker
Volume 22 August 2002	*A Coupled Ocean-Atmosphere Radiative Model for Global Ocean Biogeochemical Models* Watson W. Gregg
Volume 23 November 2002	*Prospects for Improved Forecasts of Weather and Short-term Climate Variability on Subseasonal (2-Week to 2-Month) Time Scales* Siegfried D. Schubert, Randall Dole, Huang van den Dool, Max J. Suarez, and Duane Waliser
Volume 24 July 2003	*Temperature Data Assimilation with Salinity Corrections: Validation for the NSIPP Ocean Data Assimilation System in the Tropical Pacific Ocean, 1993–1998* Alberto Troccoli, Michele M. Rienecker, Christian L. Keppenne, and Gregory C. Johnson
Volume 25 December 2003	*Modeling, Simulation, and Forecasting of Subseasonal Variability* Duane Waliser, Siegfried D. Schubert, Arun Kumar, Klaus Weickmann, and Randall Dole
Volume 26 April 2005	*Documentation and Validation of the Goddard Earth Observing System (GEOS) Data Assimilation System – Version 4* Senior Authors: S. Bloom, A. da Silva and D. Dee Contributing Authors: M. Bosilovich, J-D. Chern, S. Pawson, S. Schubert, M. Sienkiewicz, I. Stajner, W-W. Tan, and M-L. Wu
Volume 27 December 2008	*The GEOS-5 Data Assimilation System - Documentation of Versions 5.0.1, 5.1.0, and 5.2.0.* M.M. Rienecker, M.J. Suarez, R. Todling, J. Bacmeister, L. Takacs, H.-C. Liu, W. Gu, M. Sienkiewicz, R.D. Koster, R. Gelaro, I. Stajner, and J.E. Nielsen

Volume 28 April 2012	*The GEOS-5 Atmospheric General Circulation Model: Mean Climate and Development from MERRA to Fortuna* Andrea Molod, Lawrence Takacs, Max Suarez, Julio Bacmeister, In-Sun Song, and Andrew Eichmann
Volume 29 June 2012	*Atmospheric Reanalyses – Recent Progress and Prospects for the Future.* *A Report from a Technical Workshop, April 2010* Michele M. Rienecker, Dick Dee, Jack Woollen, Gilbert P. Compo, Kazutoshi Onogi, Ron Gelaro, Michael G. Bosilovich, Arlindo da Silva, Steven Pawson, Siegfried Schubert, Max Suarez, Dale Barker, Hirotaka Kamahori, Robert Kistler, and Suranjana Saha
Volume 30 December 2012	*The GEOS-iODAS: Description and Evaluation* Guillaume Vernieres, Michele M. Rienecker, Robin Kovach and Christian L. Keppenne
Volume 31 March 2013	*Global Surface Ocean Carbon Estimates in a Model Forced by MERRA* Watson W. Gregg, Nancy W. Casey and Cécile S. Rousseaux
Volume 32 March 2014	*Estimates of AOD Trends (2002-2012) over the World's Major Cities based on the MERRA Aerosol Reanalysis* Simon Provencal, Pavel Kishcha, Emily Elhacham, Arlindo M. da Silva, and Pinhas Alpert
Volume 33 August 2014	*The Effects of Chlorophyll Assimilation on Carbon Fluxes in a Global Biogeochemical Model* Cécile S. Rousseaux and Watson W. Gregg
Volume 34 September 2014	*Background Error Covariance Estimation using Information from a Single Model Trajectory with Application to Ocean Data Assimilation into the GEOS-5 Coupled Model* Christian L. Keppenne, Michele M. Rienecker, Robin M. Kovach, and Guillaume Vernieres
Volume 35 December 2014	*Observation-Corrected Precipitation Estimates in GEOS-5* Rolf H. Reichle and Qing Liu
Volume 36 March 2015	*Evaluation of the 7-km GEOS-5 Nature Run* Ronald Gelaro, William M. Putman, Steven Pawson, Clara Draper, Andrea Molod, Peter M. Norris, Lesley Ott, Nikki Prive, Oreste Reale, Deepthi

Achuthavarier, Michael Bosilovich, Virginie Buchard, Winston Chao, Lawrence Coy, Richard Cullather, Arlindo da Silva, Anton Darmenov, Ronald M. Errico, Marangelly Fuentes, Min-Jeong Kim, Randal Koster, Will McCarty, Jyothi Nattala, Gary Partyka, Siegfried Schubert, Guillaume Vernieres, Yuri Vikhliaev, and Krzysztof Wargan

Volume 37
March 2015

Maintaining Atmospheric Mass and Water Balance within Reanalysis

Lawrence L. Takacs, Max Suarez, and Ricardo Todling

Volume 38
September 2015

The Quick Fire Emissions Dataset (QFED) – Documentation of versions 2.1, 2.2 and 2.4

Anton S. Darmenov and Arlindo da Silva

Volume 39
September 2015

Land Boundary Conditions for the Goddard Earth Observing System Model Version 5 (GEOS-5) Climate Modeling System - Recent Updates and Data File Descriptions

Sarith Mahanama, Randal Koster, Gregory Walker, Lawrence Takacs, Rolf Reichle, Gabrielle De Lannoy, Qing Liu, Bin Zhao, and Max Suarez

Volume 40
October 2015

Soil Moisture Active Passive (SMAP) Project Assessment Report for the Beta-Release L4_SM Data Product

Rolf H. Reichle, Gabrielle J. M. De Lannoy, Qing Liu, Andreas Colliander, Austin Conaty, Thomas Jackson, John Kimball, and Randal D. Koster

Volume 41
October 2015

GDIS Workshop Report

Siegfried Schubert, Will Pozzi, Kingtse Mo, Eric Wood, Kerstin Stahl, Mike Hayes, Juergen Vogt, Sonia Seneviratne, Ron Stewart, Roger Pulwarty, and Robert Stefanski

Volume 42
November 2015

Soil Moisture Active Passive (SMAP) Project Calibration and Validation for the L4_C Beta-Release Data Product

John Kimball, Lucas Jones, Joseph Glassy, E. Natasha Stavros, Nima Madani, Rolf Reichle, Thomas Jackson, and Andreas Colliander

Volume 43
September 2015

MERRA-2: Initial Evaluation of the Climate

Michael G. Bosilovich, Santha Akella, Lawrence Coy, Richard Cullather, Clara Draper, Ronald Gelaro, Robin Kovach, Qing Liu, Andrea Molod, Peter Norris, Krzysztof Wargan, Winston Chao, Rolf Reichle, Lawrence Takacs, Yury Vikhliaev, Steve Bloom, Allison Collow, Stacey Firth, Gordon Labow, Gary Partyka, Steven Pawson, Oreste Reale, Siegfried Schubert, and Max Suarez

Volume 44
February 2016

Estimation of the Ocean Skin Temperature using the NASA GEOS Atmospheric Data Assimilation System

Santha Akella, Ricardo Todling, Max Suarez

Volume 45
October 2016

The MERRA-2 Aerosol Assimilation

C. A. Randles, A. M. da Silva, V. Buchard, A. Darmenov, P. R. Colarco, V. Aquila, H. Bian, E. P. Nowottnick, X. Pan, A. Smirnov, H. Yu, and R. Govindaraju

Volume 46
October 2016

The MERRA-2 Input Observations: Summary and Assessment

Will McCarty, Lawrence Coy, Ronald Gelaro, Albert Huang, Dagmar Merkova, Edmond B. Smith, Meta Sienkiewicz, and Krzysztof Wargan

Volume 47
May 2017

An Evaluation of Teleconnections Over the United States in an Ensemble of AMIP Simulations with the MERRA-2 Configuration of the GEOS Atmospheric Model.

Allison B. Marquardt Collow, Sarith P. Mahanama, Michael G. Bosilovich, Randal D. Koster, and Siegfried D. Schubert

Volume 48
July 2017

Description of the GMAO OSSE for Weather Analysis Software Package: Version 3

Ronald M. Errico, Nikki C. Prive, David Carvalho, Meta Sienkiewicz, Amal El Akkraoui, Jing Guo, Ricardo Todling, Will McCarty, William M. Putman, Arlindo da Silva, Ronald Gelaro, and Isaac Moradi

Volume 49
March 2018

Preliminary Evaluation of Influence of Aerosols on the Simulation of Brightness Temperature in the NASA Goddard Earth Observing System Atmospheric Data Assimilation System

Jong Kim, Santha Akella, Will McCarty, Ricardo Todling, and Arlindo M. da Silva

Volume 50
March 2018

The GMAO Hybrid Ensemble-Variational Atmospheric Data Assimilation System: Version 2.0

Ricardo Todling and Amal El Akkraoui

Volume 51
July 2018

The Atmosphere-Ocean Interface Layer of the NASA Goddard Earth Observing System Model and Data Assimilation System

Santha Akella and Max Suarez

Volume 52

Soil Moisture Active Passive (SMAP) Project Assessment Report for Version 4 of the L4_SM Data Product

July 2018	Rolf H. Reichle, Qing Liu, Randal D. Koster, Joe Ardizzone, Andreas Colliander, Wade Crow, Gabrielle J. M. De Lannoy, and John Kimball
Volume 53 October 2019	*Ensemble Generation Strategies Employed in the GMAO GEOS-S2S Forecast System* Siegfried Schubert, Anna Borovikov, Young-Kwon Lim, and Andrea Molod
Volume 54 August 2020	*Position Estimation of Atmospheric Motion Vectors for Observation System Simulation Experiments* David Carvalho and Will McCarty
Volume 55 February 2021	*A Phenomenon-Based Decomposition of Model-Based Estimates of Boreal Winter ENSO Variability* Schubert, Siegfried, Young-Kwon Lim, Andrea Molod, and Allison Collow